A Theory for the Surface Induced Growth of Helium Gas Bubbles in Irradiated and Annealed Copper-Boron Alloys

G.P. Tiwari[1], M. Laghate[2] and R.S. Mehrotra[3]

[1]Ram Rao Adik Institute of Technology, Vidya Nagari, Nerul, Navi Mumbai-400709, India

[2]Computer Division, Bhabha Atomic Research Centre Trombay, Mumbai-400085, India

[3]Rohini CHS, Sector 9A, Vashi, Navi Mumbai-400703, India

Corresponding author: G.P. Tiwari, Email: gyanendra.tiwari@gmail.com

Abstract

Neutron irradiated copper-boron alloys are employed to study the mutual interaction between metallic crystalline lattices and inert gases. Inert gases precipitate to form gas bubbles and their growth induces dilation of the matrix. This dilation, technically designated as swelling, affects the structural integrity of nuclear fuels during their service. The estimated enthalpy of solution of helium in copper is 5.5 eV/atom. As a Consequence, its solubility in the copper matrix is extremely poor and it cannot enter a copper based matrix via any thermo-chemical route. Hence, recourse to a nuclear reaction is taken to impregnate copper with helium. Helium is produced in situ through neutron irradiation in copper-boron alloys as a result of (n, α) nuclear reaction between boron atoms and neutrons. The characteristic feature of the growth of helium gas bubbles driven by isothermal annealing of the metallic matrix is that their rate of growth is highly sensitive to the distance of the bubbles from the external surface of the specimen. The growth of gas bubbles as a function of time and temperature is modulated by the flow of vacancies from the free surface of the specimen. A theory for the surface induced growth of helium gas bubbles in the neutron irradiated copper-boron alloys is presented here.

Keywords: Irradiation, Helium, Bubbles, Swelling, Vacancy, Diffusion

1. Introduction

The presence of helium is unavoidable in the structural materials of fission as well as fusion reactors [1-5]. The formation and growth of helium gas bubbles causes embrittlement, impairs structural stability and reduces the service life of reactor components. In view of these considerations, behavior of trapped helium in metallic systems is receiving a great deal of theoretical and experimental attention. Monte Carlo [6] and molecular dynamics [7] routines are being used to develop codes to predict the changes in mechanical properties and evolution of microstructures. These efforts are directed at evolving performance codes to establish the operational margins for the nuclear fuels [7-8].

Neutron irradiated copper-boron alloys are ideally suited to study the behavior of helium gas bubbles in crystalline matrices [9-14]. This is mainly due to the fact that residual radioactivity after irradiation and reasonable period of cooling is sufficiently low and the specimen can be safely handled outside the glove

boxes. The estimated enthalpy of solution of helium in copper is 5.5 eV/atom [15]. Such a high enthalpy of solution gives rise to extremely poor solubility limits at all temperatures, even up to the melting point. Thermo-chemical route, therefore, cannot introduce a significant amount of inert gas that is required in the study of their interaction with the host lattice. Ionic implantation [16-17], tritium decay [18-19] and the neutron bombardment of B^{10} atoms [20-21] are the three techniques which can be used to impregnate a metallic lattice with helium. Ion implantation forms bubbles in the near surface region up to a depth of few hundred nanometers. The difficulties associated with the tritium decay, which yields He_2^3, are the long time needed for its decay and hazards involved in the handling a radioactive gas. Neutrons generate in situ helium atoms through (n,α) reaction with B^{10} isotope which constitutes 18 wt% of naturally occurring boron. Hence, a nuclear reaction provides a superior alternative to create a uniform distribution of helium via boron precipitates. The nuclear reaction used to introduce helium in copper matrix is as follows:

$$B^{10} + n^1 = Li^7 + 2He^2$$

The precipitation in the form of gas bubbles and their growth is a diffusion controlled phenomenon and the bubbles coarsen progressively in size with time. The coarsening or the growth in the size of bubbles is associated with the increase in volume of the matrix. Such a dilation of the matrix due to growth of the gas bubbles located within the matrix is technically designated as swelling. In this respect, the growth of the inert gas bubbles is different from that of any solid dispersion. In the latter case, the coarsening is not accompanied by increase in the volume of the matrix. The technological importance of swelling lies in the fact that it critically affects the dimensional integrity of structural components as well as nuclear fuels and reduces their service life. A matrix containing inert gas dilates in direct proportion to the growth undergone by the gas bubbles and almost the entire increase in volume of the matrix is accounted for by the volume occupied by the coarsened gas bubbles [22-25]. In view of the low boron content and the fact that it occurs in the copper matrix in the form of precipitates, a copper-boron matrix can be considered to behave as a pure copper matrix as far as its diffusion behavior is concerned. Hence, in the subsequent sections of this paper the vacancy concentration as well as the diffusion coefficient of pure copper has been employed for the study of diffusion and growth of helium in copper-boron matrix.

It has been hypothesized earlier that vacancies originating from the external surface condense spontaneously on the surface of the gas bubbles [26-27]. The external surface induces the growth of the gas bubbles by serving as a source of vacancies. The driving force for such a spontaneous condensation of vacancies is provided by the inherent tendency of the gas trapped inside the bubble to lower its free energy through volumetric expansion [13]. In the presence of inert gas bubbles, a vacancy gradient is created between the external surface of the specimen and the interior of the matrix. The vacancies migrate from the external surface and condense on the surface of the bubbles. A theory for the growth of inert gas bubbles through deposition of vacancies on their surface is presented here. The model predicts that the rate of growth of the bubbles decreases in a progressive manner as a function of the inverse of the cube of its distance from the external surface of the specimen.

2. Deposition of Vacancies on the Surface of Gas Bubbles

If two separate gas bubbles are forced into coalescence by impingement of their surfaces, there will be a net increase in the volume provided their surfaces areas are conserved [22]. This phenomenon was

experimentally demonstrated by Barnes [28-29] in an electron microscope. The temperature gradient created by the electron beam provided the driving force. In contrast, there is a complete absence of temperature and stress gradient during the post-irradiation annealing. In these conditions, coalescence induced by the bubble migration is possible only during recrystallization of the matrix via the movement of dislocations and grain boundaries. However, this phenomenon has only a very limited role in the overall swelling of the matrix for two reasons: the bubbles greater than a few microns cannot be dragged by moving dislocations and grain boundaries and the bubbles themselves, acquired during their migration, retard their movements [30]. Hence, growth of stationary gas bubbles is possible only through the condensation of vacancies on their surfaces [26-27].

Before giving a mathematical formulation of the swelling phenomenon, it is essential to recall the characteristic features associated with swelling arising from the presence of gas bubbles filled with inert gas. Inert gas induced swelling should be distinguished from the irradiation induced void swelling [31-32]. Void swelling is a consequence of the proliferation of vacancies under intense irradiation at ambient temperatures. Inert gas atoms produced from transmutation of elements present in the matrix are known to assist in the nucleation of voids [31]. However, the inert gas atoms have little role in the further accretion of vacancies to the nuclei responsible for void swelling [32]. In contrast, the swelling originating from the inert gas atoms embedded in a solid is a high temperature phenomenon. It occurs at temperatures greater than $0.5T_m$; T_m being the melting point. This kind of swelling is a thermodynamically spontaneous process and the dilation of the matrix is fully subsumed by the volume occupied by the inert gas bubbles. The swelling driven by the inert gas bubble neither causes plastic deformation nor any change in the lattice parameter. Usually, different sections of the same specimen swell at different rates. To compare the swelling rates, swelling can be expressed as the net volume occupied by the local bubbles per unit volume of the matrix in a particular section. Alternatively, it may be also expressed as the percentage increase in the overall volume in that section of the matrix.

Under the conditions outlined above, the change in volume of a bubble, ∂V, taking place in a small interval of time, ∂t, may be expressed as [33]:

$$\frac{\partial V}{\partial t} = JA\Omega . \qquad (1)$$

In the equation (1), V and A are respectively the volume and surface area of a growing bubble, Ω is the atomic volume of the matrix, t time and *J* the flux of vacancies reaching the surface of bubble from the external surface. Equation (1) postulates that, in the absence of temperature and stress gradients, a vacancy flux can mediate inert gas induced swelling. In a crystalline matrix, only the free external surface can act as a perennial source of vacancies. To a limited extent, the grain boundaries also can serve as a source of vacancies. This is specially so for the grain boundaries having access to the external surfaces [26]. However, the line defects such as dislocations and twin boundaries would be ineffective in this regard [34]. Grain boundary route for acquisition of vacancies will be accessible only to those bubbles which are located on the grain boundary itself. Let C_{VO}^e and C_V^e respectively be the equilibrium concentration of thermal vacancies on the external surface and within the matrix. The magnitudes of C_{VO}^e and C_V^e depend only on the temperature and both of them have fixed and finite values. We expect C_{VO}^e to

be far greater than C_V^e. However, both are similar in one important respect. These are equilibrium quantities and their invariance with time is ensured by the thermodynamics since the vacancy is an equilibrium defect. Also, let D be the self-diffusion coefficient of copper in the copper-boron alloy matrix and X be the distance between the surface of the bubble and the external surface. Fick's first law for unidirectional linear diffusion is represented as [34]:

$$J = -D\frac{\partial C}{\partial X}. \tag{2}$$

The term ($\partial C / \partial X$) is the concentration gradient of the diffusing species. In the present case, growth of the bubbles is not driven by the concentration gradient of any atomic species. Here, the vacancy itself is the diffusing species.

The term ($\partial C / \partial X$) is given as below:

$$\frac{\partial C}{\partial X} = \frac{C_{VO}^e - C_V^e}{X}. \tag{3}$$

Hence,
$$J = D\frac{C_{VO}^e - C_V^e}{X}. \tag{4}$$

The negative sign gets eliminated because the sense of the direction of the bubble growth and the gradient of vacancies are in the opposite directions. Transposing and combining the equations (1) and (4), we get:

$$\frac{\partial V}{A} = D\frac{C_{VO}^e - Ce_V}{X}\Omega\partial t. \tag{5}$$

During nucleation, formation of a new phase requires the creation of new surface and spherical geometry minimizes the surface area in the formation of a nucleus. As shown in the Appendix 1, the surface area of a sphere and volume are related as follows:

$$A = \frac{V^{2/3}}{0.21}. \tag{6}$$

By substitution from equation (6) into equation (5), we have:

$$0.21V^{-2/3}\partial V = D\frac{C_{VO}^e - C_V^e}{X}\Omega\partial t. \tag{7}$$

The growth of the gas bubbles is a diffusion controlled phenomenon [17-18] and the kinetics of the bubble growth is governed by the diffusion coefficient mentioned above. Presently, we are interested in the behavior of bubbles at a constant temperature in a compositionally homogenous matrix. As a result, the parameter D in the equation (7) can be treated as a constant. In order to facilitate the integration, we make the following substitution [34]:

$$X = \lambda\sqrt{t}\ . \qquad (8)$$

λ is a constant independent of X and t. Substituting for X in the equation (7) from equation (8) and integrating, we get:

$$0.21\int_{V_o}^{V_f} V^{-2/3}\partial V = D.\Omega.\frac{C_{VO}^e - C_V^e}{\lambda}\int_0^t t^{-1/2}\partial t \qquad (9)$$

Here, V_0 and V_f are respectively the volumes of the bubble at the start of annealing ($t = 0$) and at the end of annealing period (t). As discussed above, the terms outside the integral in the right hand side of equation (9) are invariant at any fixed temperature and composition. Therefore, integrating the equation (9), we get:

$$(V_f^{1/3} - V_0^{1/3}) = Kt^{1/2}\ . \qquad (10)$$

K is a constant defined as below:

$$K = 3.23\frac{D\Omega(C_{VO}^e - C_V^e)}{\lambda}\ . \qquad (11)$$

At the start of annealing ($t = 0$), when the bubbles are submicroscopic, the net volume occupied by them is negligibly small. Hence, we may safely take $V_O \approx 0$. Substituting for λ from equation (8), we finally obtain:

$$V_f = [3.23D(C_{VO}^e - C_V^e)\Omega t]^3(1/X^3)\ . \qquad (12)$$

Equation (12) gives the average size of the bubbles after annealing at any point (X) in the matrix as a function of annealing time and its distance from the free surface. The size of the bubble at different cross sections of the specimen varies as the cube of the inverse of its distance from the surface. However, our aim is to evaluate the net dilation or the local swelling as a function of the distance from the surface in the matrix on account of growth experienced by the gas bubbles after its nucleation. To achieve this, the parameter (V_f) is multiplied by the total number of the bubbles to obtain the net dilation of the matrix caused by formation and growth of the gas bubbles. Let n be the density of the bubbles defined as the number of the bubbles per unit volume of the matrix at the end of nucleation stage and the initiation of the growth process. n is invariant with respect to X, the assumption being that the rate of nucleation is uniform through the specimen. The assumption is justified since the density of nucleation at any point in the matrix depends upon the temperature, microstructure and the concentration of helium which are unaltered across the entire cross section of the specimen. Hence, the swelling per unit volume of the specimen caused by the growth of the gas bubbles as function of its distance (X) from the surface can be expressed as,

$$\frac{\Delta V}{V} = n.V_f = n[3.23D(C_{VO}^e - C_V^e)\Omega.t)]^3(1/X^3) \qquad (13)$$

Thus, $\frac{\Delta V}{V}$ represents the fractional increase in the volume of the matrix originating from the growth of gas bubbles. It is used subsequently in the analysis of the data given in the tables 1 and 2. In percentage terms, the swelling is given by $\frac{\Delta V}{V} \times 100$.

3. Discussion

The present paper deals with the growth of helium bubbles during isothermal annealing and here the atoms in the host lattice do not undergo any kind of displacement. The possible mechanisms which can assist the growth of helium gas bubbles in the temperature range where displacement damage can be neglected are (a) gaseous diffusion and absorption in the existing bubbles, (b) random bubble migration and coalescence via surface diffusion (c) Oswald ripening due to helium fluxes driven by the differences in the thermal equilibrium helium concentrations in the vicinity of small and large bubbles [2]. In the absence of vacancy super-saturation in the host matrix, gas bubbles grow via inflow and deposition of vacancies from the free surface which envelopes the body of the specimen. In an earlier paper [26], experimental evidence regarding the growth and calescence of stationary immobile bubbles through vacancy deposition was presented. In this situation, changes in the size of bubbles are governed by the following equation [13]:

$$NRT \ln\left(\frac{V_f}{V_0}\right) = \gamma(A_f - A_o). \qquad (14)$$

In the equation (14), N is the number of moles of gas within the bubble cavity, V_f and V_o are the initial and final volumes of the bubble, A_f and A_o are the initial and final surface areas of the bubble and γ is the surface tension of the matrix. The equation shows that the energy for the creation of extra surface in the course of bubble growth is provided by an increase in the volume of the gas. In this context, Dayton et al. [35] showed that the inert gas release as well as the swelling decreased substantially after irradiation and annealing of coated uranium dioxide and mixed uranium-thorium oxide fuel microspheres. These authors also reported that if the coating developed cracks and thus exposed the outer surface of the underlying matrix, the swelling increased substantially. Thus the surface induced growth of gas bubbles is not specific only to helium but to all types of inert gas bubbles which are trapped inside any crystalline matrix. The phenomenon of breakaway swelling and the formation of pinholes in helium implanted metallic specimen can also be explained with the help of equation (14). Since the gas trapped inside a gas bubble will try to lower its free energy through expansion, the bubble growth will continue in an unhindered manner till the bubble transforms into a crack and gas escapes into the atmosphere. Absorption of radiation induced super-saturated vacancies within the grains and the migration of free vacancies from the surface can continue unabated as the energy released by the expansion of the helium gas trapped inside the bubble is higher than the energy needed for the surface increase during its growth.

In these circumstances, the bubble growth can continue till the gas escapes due to the formation of crack or pinhole. At high burn up, rim effect in metallic uranium as well as oxide fuel is associated with the formation of fine grains and highly pressurized gas bubbles in peripheral regions on the fuel pellet [31]. In principle, the bubbles in the peripheral regions may also grow by accepting vacancies from free surface. This kind of bubble growth followed by their coalescence may lead to the formation of cracks and release of fission gases into the plenum space. It is, therefore, suggested that in any model designed to predict/estimate inert gas induced swelling, the possibility of bubble growth through the migration and deposition of vacancies from the external surface should be carefully examined.

In an earlier publication, present model was applied to the data on swelling as a function of time and a satisfactory agreement between the rate of bubble growth predicted by the theory and the experiments was observed [33]. Presently, equation (13) will be applied to dada on the variations in the growth of gas bubbles as we traverse from the external surface towards the center of the specimen. The results of Pati and Barrand [9] are suitable for the application of present model because of the availability of Figs.1 and 2, which show longitudinal and transverse sections of an irradiated and annealed copper boron alloy. These figures clearly bring out the fact that bubbles near the surface of the specimen experience higher growth than the bubbles located deeper inside. There will a time gap between the moment when a vacancy leaves the free surface and the time it reaches the bubble. This time will be relatively shorter if the distance travelled by the vacancy to reach the bubble is smaller and vice-versa. Unlike Pati and Barrand [9], most of the authors (see for example; Greenwood [23] and Mustelier et al. [36]) have been content to display the differences in the rate of bubble sizes in the near surface region and in the sections away from the surface by using two different figures. The demonstration of progressive decrease in the size of the gas bubbles as we move away from the surface to the deeper section of the specimen in a single frame is required for the application of the present model to the experimental results. Dark areas in the Figs. 1 and 2 represent the areas occupied by gas bubbles which are bared after sectioning. The model for the bubble growth presented here assumes a spherical geometry during the initial stages of their growth. A careful examination of the microstructures shown in the Figs. 1 and 2 suggests that bubbles indeed have a spherical geometry to start with. The irregular shapes are obtained as a result of the coalescence between adjacent bubbles. Barnes [28-29] has shown that the coalescence of the bubbles conserves the surface area of the bubbles. Hence, the net area available for vacancy deposition remains unchanged even if the bubbles acquire irregular shapes subsequently through coalescence.

The data were extracted from Figs.1 and 2 using software developed by one of the authors and recorded in the Tables 1 and 2 respectively. The area fraction occupied by the gas bubbles is converted into volume fraction with the use of the relation $V = (Area)^{3/2}$. The data in the Tables 1 and 2 for volume fraction of the bubbles as a function of cube of the reciprocal of distance as measured from the external surface $(1/X^3)$ are plotted in Figs. 3 and 4 respectively. As expected from the equation (11), there is a steep fall in the volume fraction of gas bubbles as we move away from the surface. The most significant feature of the Figs. 3 and 4 is that the rate of bubble growth in the near surface region (marked as region 1 in the figures) is different from those located farther away from the surface (marked as the region 2). The rate of the bubble growth, indicated by the slopes of the curve from the two regions, is faster in the region 2 as compared to that in region 1. The interesting and intriguing aspect of the Figs. 3 and 4 is that despite the relatively slower rate of growth, overall volume of the bubbles in the near surface region is higher

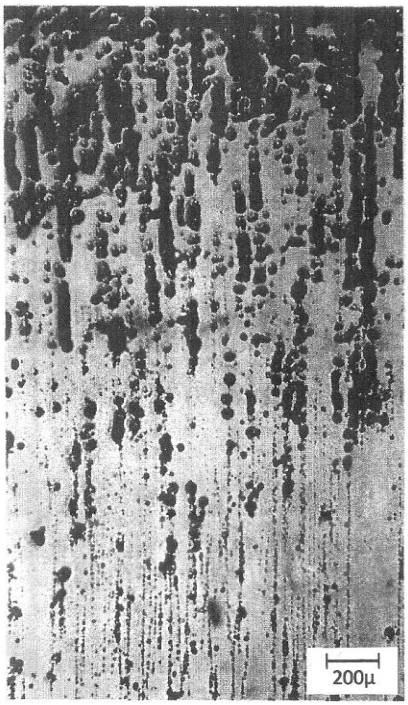

Fig.1 Microstructure of the longitudional cross section of irradiated and annealed cylindrical wire Cu/0.085wt% B alloy specimen in as-polished condition [1].

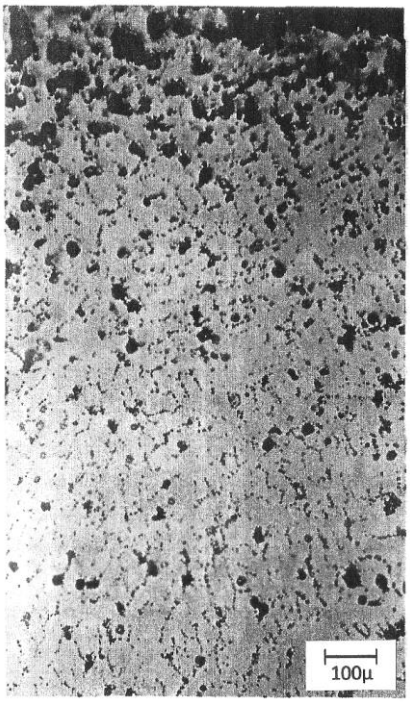

Fig.2. Microstructure of the transverse cross section near the midlength of irradiated and annealed cylindrical wire copper-boron alloy specimen in as-polished condition [1].

in the sections located deeper inside where the growth rate is higher. The reasons for the differences in the growth rates of bubbles in the two regions are discussed below.

3.1 Growth Rate in Region 1

As shown in the Appendix 2, the slope of the plot of volume fraction of bubbles ($\Delta V/V$) against the cube of the reciprocal of the distance from the surface ($1/X^3$) estimated on the basis of the equation (13) is equal to $4.84x10^{-10}$ cm^3 .To obtain the magnitude of swelling in percentage terms, this should be multiplied by 100. This yields a value of $4.84\times10^{-8}\,cm^3$. Actual values of the slopes in the region 1 for both Fig.3 and Fig.4 are equal to $9x10^{-8}$. The calculated value is 1.96 times higher than the experimental value. In the Appendixes given at the end, various possible sources of error are identified and their contribution to total error in the value of slope (S) are estimated. It is found that total error introduced by the uncertainties in the magnitudes of the parameters associated with S amounts to one hundred percent. If we combine it with the difference in calculated and experimental, the overall difference in experimental and theoretical values of S sums up to 200%. We feel this type of agreement validates our model.

S. No.	X	$1/X^3$	Area Fraction	Volume Fraction $(\frac{\Delta V}{V})$
1	0.01032	909910	0.708006	0.595738
2	0.012364	529120	0.691713	0.575293
3	0.015417	272878	0.675419	0.555086
4	0.020639	113739	0.658728	0.534637
5	0.031211	32891.6	0.642037	0.514h446
6	0.05185	7173.76	0.604211	0.469659
7	0.071986	2680.75	0.51455	0.369098
8	0.093884	1208.43	0.305312	0.1687
9	0.117041	623.722	0.2697	0.140062
10	0.139442	368.825	0.229033	0.109609
11	0.160836	240.352	0.168162	0.068959
12	0.181224	168.017	0.177621	0.074859
13	0.20136	122.484	0.102149	0.032648
14	0.221244	92.3387	0.156665	0.06201
15	0.240625	71.7755	0.11451	0.038749

Table 1: Data Analysis for Image of Fig.1

(The data is up to 6 significant digits)

S. No.	X	$1/X^3$	Area Fraction	Volume Fraction $(\frac{\Delta V}{V})$
1	0.007674	2212930	0.504333	0.358159
2	0.01	1000000	0.372598	0.227437
3	0.015	296296	0.357069	0.213367
4	0.025223	62318.2	0.268039	0.13877
5	0.04252	13007.9	0.226304	0.107656
6	0.060258	4570.37	0.138166	0.051357
7	0.078688	2052.47	0.13162	0.047751
8	0.097558	1076.99	0.125665	0.044547
9	0.116365	634.648	0.101336	0.032259

Table 2: Data Analysis for Image of Fig.2

(The data is up to 6 significant digits)

It should also be mentioned here the data on volume occupied by the bubbles used in this paper were taken from a single cross section of the specimen. A minimum of five sections should be analyzed to get more representative values of the volume of the bubbles. However, the present article does serve to delineate the role of the free surface and diffusion of vacancies in the inert gas induced swelling of the crystalline solids.

3.2 Growth in the Region 2

Here the growth rates are higher by about two orders of magnitudes. The preferential location of bubbles along the grain boundaries in this region (see Fig.2) is a signal for the role of grain boundaries in their growth. To consider the growth of the gas bubbles located at the grain boundaries, the equation (13) is transformed as below:

$$V_f^{gb} = n_{gb}\kappa[3.23D_{gb}(C_{VO}^e - C_V^e)\Omega t)]^3(1/X^3)\,. \qquad (15)$$

V_f^{gb} is the net volume of the bubbles per unit volume of the matrix located at grain boundaries at a distance of X from the surface, n_{gb} is the density of bubbles per unit of grain boundary volume, κ is the average fraction of atoms located at the grain boundaries and D_{gb} is the grain boundary diffusion coefficient. When the lattice as well as grain boundaries are taking part in diffusion, the effective diffusion coefficient, D_{eff} , is given by,

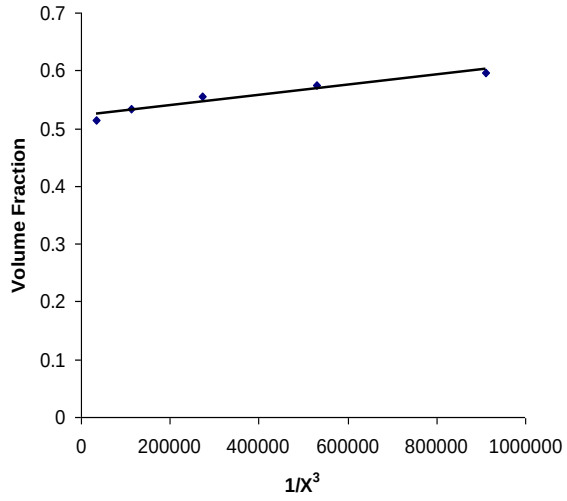

Fig.3 (a): Volume Fraction of bubbles as a function of $1/X^3$ for the first five data given in table 1. The data have an error band of 5%. The equation for least squares fit line is:

$$y = 9\text{x}10^{-8}\, x + 0.5226$$

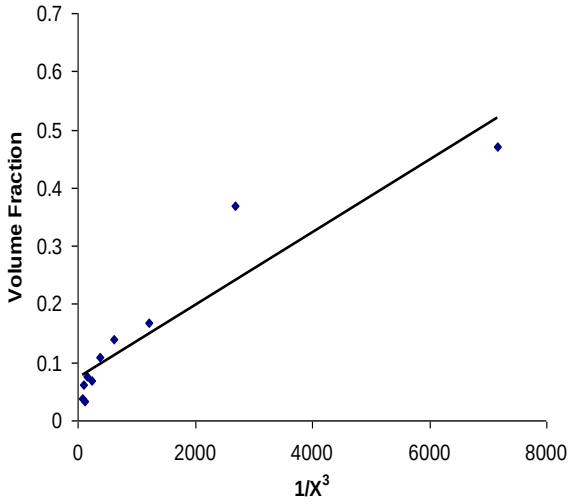

Fig.3 (b): Volume Fraction of bubbles as a function of $1/X^3$ for the last ten data given in table 1. The data have an error band of 5%. The equation for least squares fit line is:

$$y = 6\text{x}10^{-5}\, x + 0.0739$$

$$D_{eff} = D(1-\kappa) + \kappa D_{gb}. \qquad (16)$$

To obtain an estimate of κ , we make an imaginary transverse section across the specimen surface. Let μ and δ be the average grain size and the width of the grain boundary. This imaginary section will be intercepted by a grain boundary across its length at an interval of μ. Hence, we will come across an atom located at the grain boundary after a distance of μ. Further, if a is the lattice parameter, then we have one atom at the lattice site after an interval of a. The value of μ given by Pati and Barrand [9] is 0.034 cm. Therefore, κ is given by,

$$\kappa = \frac{(1/\mu)}{(1/a)} = \frac{a}{\mu} = \frac{3.6075x10^{-8}}{3.4x10^{-3}} = 1.061x10^{-5} \qquad (17)$$

Substituting the value of κ in the equation 15, we obtain,

$$D_{eff} = D(1-1.06x10^{-5}) + 1.06x10^{-5} D_{gb}. \qquad (18)$$

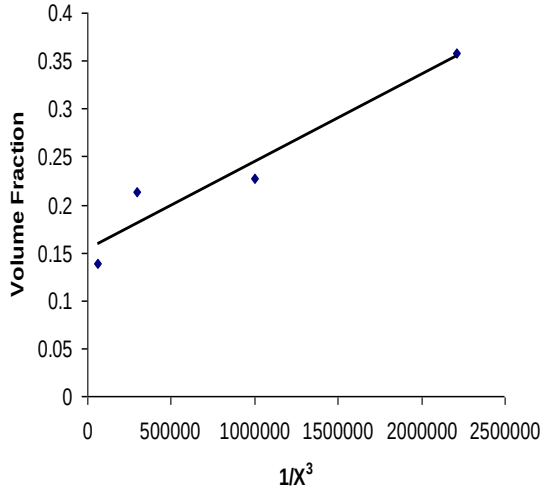

Fig.4 (a): Volume Fraction of bubbles as a function of $1/X^3$ for the first four data given in table 2. The data have an error band of 5%. The equation for least squares fit line is:

$$y = 9x10^{-8}\, x + 0.1532$$

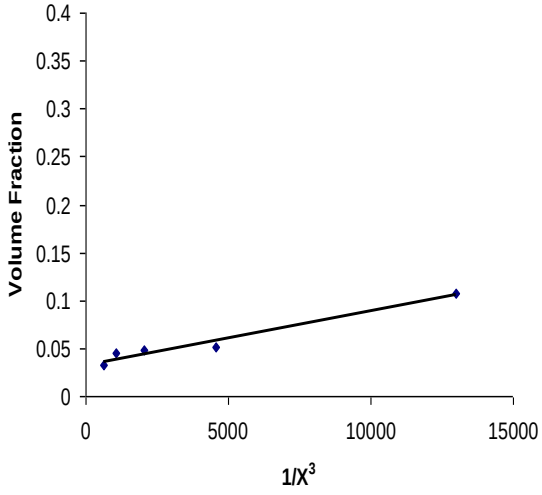

Fig.4 (b): Volume Fraction of bubbles as a function of $1/X^3$ for the last five data given in table 2. The data have an error band of 5%. The equation for least squares fit line is:

$$y = 6x10^{-6}\, x + 0.0326.$$

Since the value of κ is small, its influence on the role of lattice diffusion as it relates to the bubble growth is negligible. However, it reduces the net contribution of grain boundaries to the overall growth of the gas bubbles cross-sectional area available for the bubble growth by a factor of 10^5. As we do not have any specific information regarding the density of nucleation along the grain boundaries, it is not possible to make a quantitative assessment of the swelling induced by the growth of bubbles located in the grain boundaries. However, the higher rate of growth of bubbles in the second region can be attributed to the fact that grain boundary diffusion coefficient is 10^4 times greater than the lattice diffusion coefficient. Despite higher diffusion rates, the smaller swelling in the second region is due to the reduction in the cross sectional area available for the bubble growth.

Summary

A theory is presented to explain the gradation observed in the growth of helium gas bubbles in an irradiated and annealed copper-boron alloy as we traverse from the surface to the interiors of the specimen. The growth in the gas bubbles is caused by the spontaneous deposition of vacancies on their surface. The external surface constitutes a perennial source of vacancies and a vacancy gradient is created between the open external surface and the bubbles. The kinetics of bubble growth is controlled by the rate of diffusion of vacancies in the matrix. The theory satisfactorily explains the microstructural evidence on the gradual decrease in the growth of bubbles from surface to the interiors of the irradiated and annealed copper–boron alloy.

REFERENCES

1. C.M. Schaldach and W.G. Wolfer, in: M.L Grossbeck, T.R. Allen, R.G.Lott, and A.S. Kumar (Eds.), Effects of Radiation on Materials: 21st International Symposium, ASTM STP 1447, ASTM International, West Conshohocken, PA, 2004, p.105.

2. H.Trinkaus and B.N. Singh, J. Nucl. Mater. 323 (2003) 229-242.

3. K. Morishita and R. Sugano, J. Nucl. Mater. 353 (2006) 52-65.

4. R. E. Stoller, P. J. Maziasz, A. F. Rowcliffe, , J. Nucl. Mater. 155-157 (1988) 1328-1334.

5. P.I. Lane and P.J. Goodhew, Phil. Mag. A. 48 (1983) 965-986.

6. T.Suzudo, H. Kaburaki and E. Wakai, Joint International Tropical Meeting on Mathematics & Computation and Supercomputing in Nuclear applications (MNC+SNA), Monterey, California, on CD-ROM, American nuclear society, 2007.

7. M.R. Tonks, S.B. Biner, P.C.Millett and D.A. Andersson, Joint International Tropical Meeting on Mathematics & Computation and Supercomputing in Nuclear applications (MNC+SNA), Sun Valley, Idaho, on CD-ROM, American nuclear society, 2013.

8. P.V. Ufflen, G. Pstoren, V.D. Marcello and L. Luzzi, Nucl. Engg. and Tech. 43 (2011), 477-488.

9. S.R. Pati and P. Barrand, J. Nucl. Mater. 31 (1969), 117-120.

10. P. Vela and V. Russell, J. Nucl. Mater. 19 (1966) 312-326.

11. P. Vela and V. Russell, J. Nucl. Mater. 19 (1966) 327-340.

12. G.P. Tiwari and J Singh, J. Nucl. Mater. 172 (1990)114-122.

13. G.P. Tiwari and J. Singh, J. Nucl. Mater. 195 (1992) 205-215.

14. S.F. Pugh (Ed.), Proceedings of the Harwell Consultants' Symposium on Rare Gases in Metals and Alkali Halides, Harwell, U.K., 1979, Rad. Effects 53 (1979) 1980.

15. D.E. Rimmer and A.H. Cottrell, Phil. Mag. 2 (1957) 1345-1353.

16. G.J. Thomas and W Bauer, Radiation Effects, 17 (1973) 221-234.

17. K. Farell and N.H. Packan, J. Nucl. Mater. 85-86 (1979) 683-686.

18. C.G. Chen, H.K. Birnbaum and A. B. Jhonson Jr., J. Nucl. Mater. 79 (1979) 128-134.

19. W. Jager, R. Lasser, T. Schober and G.J. Thomas, Radiation Effects. 78 (1983) 165-176.

20. R. Nagasaki,S. Ohashi, S. Kawa and Tsuno, J. Nucl. Sci. and Tech. 8 (1971) 546-552.

21. B. Glam, S. Eliezer, D. Moreno and D. Eliezer, J. Nucl. Mater. 392 (2009) 413-419.

22. G.W. Greenwood and A.J. Boltax, J. Nucl. Mater. 5 (1962) 234-240.

23. G.W Greenwood, J. Nucl. Mater. 6 (1962) 26-34.

24. I.J. Hastings and R.L. Stoute, J. Nucl. Mater. 37 (1970) 295-302.

25. T.J. Heal, Proceedings of Third Geneva Conference on Peaceful Uses of Atomic Energy, 1964, Discussion on Paper A/Conf. 28/P/560.

26. G.P. Tiwari and J. Singh, J. Nucl. Mater. 185 (1991) 224-230.

27. G.P. Tiwari, J. Nucl. Mater. 232 (1996) 119-124.

28. R.S. Barnes, UKAEA Report AERE-R3162, 1959.

29. R.S. Barnes, J. Nucl. Mater. 11 (1964) 135-148.

30. M.W. Thompson, Defects and Radiations in Metals, Cambridge University Press (1969),p.354.

31. A.D. Brails ford and R. Bullough, J. Nucl. Mater. 44 (1972) 121-126.

32. L.K. Mansur, Nucl. Tech. 40 (1978) 5-34.

33. G.P. Tiwari and E. Ramadasan, Proceeding of 14th International Conference on Nuclear Energy (ICONE 14), on CD-ROM, ASME, Miami, Florida, USA, July 14-17, 2005.

34. H. Mehrer, Diffusion in Solids, Springer-Verlag, Berlin (2007), p.40.

35. R. W. Dayton, W.V. Goeddel and W.O. Harms, Proceedings United Nations Organization and Int. Conf. on Peaceful Uses of Atomic Energy, USA, paper no. p/250 (1958) p.538.

36. J.P. Mustelier, H. Makailoff, J.L. Ratier, D. Gondal and J. Bloch, in: D.J. Littler (Ed.), Properties of Reactor Materials and The Effects of Radiation Damage in Materials, Butterworths, London, 1962, p.359.

37. D. Gupta, in: D. Gupta (Ed.), Diffusion Processes in Advanced Technological Materials, William Andrew, NY, 2005, p.3.

38. P. Erhart, in: H. Ullmaier (Ed.), Atomic Defects in Metals, Landolt- Bornstein New Series, Vol. 25, Springer-Verlag, 1991, p.88.

39. H.P. Bonzel and N.A. Gjostein, Phys. Status. Solidi 25 (1968) 229-222.

APPENDIX-1

The relation between the surface area and volume of a sphere can be obtained as follows. As a function of radius of the sphere, the two quantities are:

$$A = 4\pi r^2 \text{ and } V = \left(4/3\right)\pi r^3 .$$

Therefore, we obtain, $$A = (4\pi)\left(3/4\pi\right)^{2/3} V^{2/3}.$$

Or $$A = 4.837V^{2/3} \qquad \text{(A1)}$$

APPENDIX-2

Calculation of slope of the plot of volume fraction of bubbles as a function of $1/X^3$

The equation (13) forms the basis of the plots of volume V against the cube of reciprocal of distance from the surface ($1/X^3$). The equation is,

$$V_f = n[3.23D(C_{VO}^e - C_V^e)\Omega t)]^3 (1/X^3) \qquad \text{(A2)}$$

Hence, the slope S of the plot of V_f versus $1/X^3$ is given by,

$$S = n[3.23(D(C_{VO}^e - C_V^e)\Omega t]^3 \qquad \text{(A3)}$$

D is the self-diffusion coefficient of copper, representing diffusion of copper in its own lattice via vacancy mechanism. Pati and Barrand [9] used spectrographically pure copper and presence of 0.085 wt% of boron will not affect self-diffusion property of the matrix in any significant manner. Hence, the self-diffusion coefficient of copper measured by standard radioactive tracer technique can be used to obtain

the value of D. Reliable data on self-diffusion coefficient [37] and vacancy formation energy [38] in copper are available. The values of these parameters at the annealing temperature 1263 K are given below:

1. Self-diffusion Coefficient D

At 1263 K, $$D = 0.20 Exp\left[-47000 \Big/ (1.987 x 1263) \right] \text{ cm}^2/\text{sec.}$$

$$= 1.47 x 10^{-9} \text{ cm}^2/\text{sec.}$$

2. Vacancy concentration per unit volume C_V^e

C_V^e = (Probability of vacancy formation at any lattice site) x (No. of copper atoms per unit volume)

= (Vacancy concentration per unit volume) x (No. of copper atoms per unit volume)

Activation energy for vacancy formation in copper is 23.07 kCal/g.mol.

Hence, $$C_V^e = \left[Exp\left(-\frac{23.07 x 10^3}{1.987 x 1263} \right) \right] \left[\frac{(AvogadroNumber)(Density_{Copper})}{AtomicWeight_{Copper}} \right]$$

$$= \left[Exp\left(-\frac{23.07 x 10^3}{1.987 x 1263} \right) \right] \left[\frac{(6.023 x 10^{23})(8.96)}{63.54} \right]$$

$$= (1.0177 x 10^{-4}) x (8.4932 x 10^{22})$$

$$= 8.644 x 10^{19}$$

3. Vacancy concentration at the surface C_{VO}^e

To our knowledge, information regarding the magnitude of C_{VO}^e the vacancy concentration on the surface is not available in literature. We have tried to obtain the value of this parameter from the data on surface diffusion in copper reported by Bonzel and Gjostein [39]. As discussed above, diffusion parameters for pure copper are being used in present calculation. According to these authors [36], surface diffusion coefficient of copper (D_s), in the temperature range 773-1233 K, is given by the following equation:

$$D_s = 0.26 \exp\left(-\frac{80.6 kJ/mol}{RT} \right) \qquad \text{(A4)}$$

Beyond this temperature range there is a steep rise in activation energy, possibly arising from vapor phase transport mechanism. We treat the activation energy in the equation (A4) as a composite quantity representing vacancy formation and migration energies for surface diffusion in pure copper to arrive at

the value of C_{VO}^{e}. This is achieved by fixing the ratio of vacancy migration and formation energies as it relates to surface diffusion in copper. The values of the ratio of vacancy formation to vacancy migration energies in metallic systems [38] are given below:

(i) FCC and HCP: 1.0 - 1.8

(ii) BCC transition metals: 2.1 -4.9

(iii) BCC alkali metals: 8.9 - 12.6

The data given above suggest that the ratio of vacancy formation to migration energy rises rapidly as we move from closed packed lattices to open structures. We surmise that the vacancy formation energy at the free surface in copper can be taken to be approximately 85% of activation energy for surface self-diffusion, the rest being for the migration of the vacancy. Hence, the magnitude of C_{VO}^{e} may be expressed as,

$$C_{V0}^{e} = \left[Exp\left(-\frac{(0.85x80.6/4.18)10^{3}}{1.987x1263} \right) \right] \left[\frac{(Avogadro's\ Number)(Density_{Copper})}{AtomicWeight_{Copper}} \right]$$

$$= (1.4576x10^{-3})x(8.4932x10^{22}) .$$

$$= 1.238x10^{20}$$

4. Number of helium gas bubbles per unit volume n

Pati and Barrand [9] have not provided any estimate of the parameter n, the number of helium gas bubbles in the swelled volume of copper matrix. As shown below, the data on volumetric swelling given in their paper can be used to get an estimate of this parameter.

The expression used for calculating the value of n is,

$$n = \frac{\pi\left[\frac{D_2^2 - D_1^2}{4}\right]h}{\left(4/3\right)\pi\left(\frac{d}{2}\right)^3 \pi(\frac{D_1^2}{4}).h} \qquad \text{(A5)}$$

where, D_1 and D_2 are sample diameters before and after swelling, h is the length of the swelled region and d is the average diameter of a single bubble.

Original diameter of the specimen = $0.5cm$

Average of the increase in diameter at the two end faces of the specimen = $0.055cm$

Average length of swelled region at the ends of the sample = $15x10^{-2}$ cm

Average diameter of the bubbles = $3.5x10^{-3}cm$

Swelling per unit volume = (Net swelling/original volume of the swelled region)

$$= \frac{\pi[(0.555/2)^2 - (0.5/2)^2]x1.5x10^{-3}}{\pi[[(0.5/2]^2 x1.5x10^{-3}}$$

n = Swelling per unit volume / Volume of a single bubble

$$= \frac{\pi[(0.555/2)^2 - (0.5/2)^2]x1.5x10^{-3}}{(4/3)\pi[(3.5/2)x10^{-3}]^3 x\pi[(0.5/2)^2]x1.5x10^{-3}]}$$

$$= 1.23x10^7$$

5. <u>The magnitude of other terms in the equation (A2)</u>

5.1 Atomic volume of copper Ω

Ω = (volume of a unit cell of copper/ number of atoms per unit cell of copper)

$$= \left(3.6149\ x10^{-8}\right)^3 / 4$$

$$= 1.18x10^{-23}$$

5.2 Period of annealing

It is the time of bubble growth as used by Pati and Barrand [9], i.e., $5.18x10^5$ sec.

<u>Calculation of the value of slope *S*</u>

Values of parameters derived in the sections 1-5 above can be used to calculate the value of slope, S, using equation (A2) as below:

$$S = n[3.23D(C_{VO}^e - C_V^e)\Omega.t]^3$$

$$= 1.29x10^7[3.23x1.47x10^{-9}(1.46x10^{-3} - 1.0177x10^{-4})8.4932x10^{22}x1.18x10^{-23}x5.18x10^5]^3$$

$$= 4.84x10^{-10}$$

APPENDIX-3.

3.1 Evaluation of error in the estimation of n

Equation (A2) used for calculating the value of n is,

$$n = \frac{\pi\left[\frac{D_2^2 - D_1^2}{4}\right]h}{\left(4/3\right)\pi\left(\frac{d}{2}\right)^3 \pi(\frac{D_1^2}{4}).h}$$

Accordingly the magnitude of error in n can be estimated from using standard error propagation procedure as follows-

$$\frac{\delta n}{n} = \sqrt{4\left(\frac{\delta D_2}{D_2}\right)^2 + 4\left(\frac{\delta D_1}{D_1}\right)^2 + \left(\frac{\delta h}{h}\right)^2 + 9\left(\frac{\delta d}{d}\right)^2} \qquad \text{(A6)}$$

We assume that the error in the values of various parameters given by Pati and Barrand [9] and used in estimation of *n* does not exceed 10%. Thus, we get:

$$\frac{\delta n}{n} = \sqrt{4(0.1)^2 + 4(0.1)^2 + (0.1)^2 + 9(0.1)^2}$$

$$= 0.1\sqrt{18}$$

$$= 0.425$$

So, the error in the value of *n* calculated above is likely to be 42.5%.

3.2 The confidence level of estimated value of the parameter S is established by use of the the error propagation formalism for as follows-

$$\frac{\delta S}{S} = \left[\sqrt{\left(\frac{\delta n}{n}\right)^2 + 3\left(\frac{\delta D}{D}\right)^2 + 3\left(\frac{\delta C_{V0}^e}{C_{V0}^e}\right)^2 + 3\left(\frac{\delta C_V^e}{C_V^e}\right)^2 + 3\left(\frac{\delta \Omega}{\Omega}\right)^2 + 3\left(\frac{\delta t}{t}\right)^2}\right] \qquad \text{(A7)}$$

The possible errors for each of the parameters in the above expression are given below.

1. The estimation of error in *n* has already been carried out using equation (A6).
2. The maximum possible error in magnitudes of self-diffusion coefficient, *D*, and vacancy concentration as used here is assumed to be 10% .
3. We surmise that the possible error in the vacancy concentration at the surface may be 50%.
4. The error in the value of Ω is negligible and hence is ignored.

5. We surmise that the maximum possible error in measurement of annealing time *t* could not exceed 5 minutes over a period of 144 hours. This gives the error value in *t* as 0.06% and it can also be ignored.

The estimated error in the value of slope is, therefore, given as:

$$\frac{\delta S}{S} = \left[\sqrt{42.5^2 + 3x10^2 + 3x50^2 + 3x10^2}\right]$$

$$= 99.53\% . \approx 100\%.$$